

Light Water Reactor Sustainability Program

High Neutron and Gamma dose effects on Calcium Silicate Deuterate

Paula Bran Anleu
Joerg Neuefeind
Hyeonseok Jee
Nishant Garg
Yann Le Pape
Elena Tajuelo Rodriguez



July 2024

U.S. Department of Energy
Office of Nuclear Energy

DISCLAIMER

This information was prepared as an account of work sponsored by an agency of the U.S. Government. Neither the U.S. Government nor any agency thereof, nor any of their employees, makes any warranty, expressed or implied, or assumes any legal liability or responsibility for the accuracy, completeness, or usefulness, of any information, apparatus, product, or process disclosed, or represents that its use would not infringe privately owned rights. References herein to any specific commercial product, process, or service by trade name, trade mark, manufacturer, or otherwise, does not necessarily constitute or imply its endorsement, recommendation, or favoring by the U.S. Government or any agency thereof. The views and opinions of authors expressed herein do not necessarily state or reflect those of the U.S. Government or any agency thereof.

DOCUMENT AVAILABILITY

Online Access: US Department of Energy (DOE) reports produced after 1991 and a growing number of pre-1991 documents are available free via <https://www.osti.gov>.

The public may also search the National Technical Information Service's [National Technical Reports Library \(NTRL\)](#) for reports not available in digital format.

DOE and DOE contractors should contact DOE's Office of Scientific and Technical Information (OSTI) for reports not currently available in digital format:

US Department of Energy
Office of Scientific and Technical Information
PO Box 62
Oak Ridge, TN 37831-0062
Telephone: (865) 576-8401
Fax: (865) 576-5728
Email: reports@osti.gov
Website: www.osti.gov

This report was prepared as an account of work sponsored by an agency of the United States Government. Neither the United States Government nor any agency thereof, nor any of their employees, makes any warranty, express or implied, or assumes any legal liability or responsibility for the accuracy, completeness, or usefulness of any information, apparatus, product, or process disclosed, or represents that its use would not infringe privately owned rights. Reference herein to any specific commercial product, process, or service by trade name, trademark, manufacturer, or otherwise, does not necessarily constitute or imply its endorsement, recommendation, or favoring by the United States Government or any agency thereof. The views and opinions of authors expressed herein do not necessarily state or reflect those of the United States Government or any agency thereof.

Nuclear Energy and Fuel Cycle Division
Light Water Reactor Sustainability Program
M2LW-24OR0403033

**HIGH NEUTRON AND GAMMA DOSE EFFECTS ON CALCIUM SILICATE
DEUTERATE**

Paula Bran Anleu
Joerg Neufeind
Hyeonseok Jee
Nishant Garg
Yann Le Pape
Elena Tajuelo Rodriguez

July 2024

Prepared by
OAK RIDGE NATIONAL LABORATORY
Oak Ridge, TN 37831
managed by
UT-BATTELLE LLC
for the
US DEPARTMENT OF ENERGY
under contract DE-AC05-00OR22725

CONTENTS

CONTENTS.....	iii
LIST OF FIGURES	iv
LIST OF TABLES	iv
ABBREVIATIONS	v
ACKNOWLEDGMENTS	vi
EXECUTIVE SUMMARY	vii
1. INTRODUCTION	1
1.1 MOTIVATION OF THE STUDY	1
1.2 EFFECTS OF GAMMA RAYS AND NEUTRONS ON CEMENT AND CEMENT HYDRATES	2
1.3 STRUCTURE AND MECHANICAL PROPERTIES OF C-S-H	3
2. SAMPLE SYNTHESIS	4
3. IRRADIATION DETAILS.....	4
4. EXPERIMENTAL DETAILS FOR POSTIRRADIATION EXAMINATION	7
4.1 THERMAL ANALYSIS.....	7
4.2 X-RAY DIFFRACTION.....	8
4.3 NEUTRON PAIR DISTRIBUTION FUNCTION ANALYSIS.....	8
5. RESULTS AND DISCUSSION.....	9
5.1 THERMAL ANALYSIS.....	9
5.2 X-RAY DIFFRACTION.....	10
5.3 NEUTRON PAIR DISTRIBUTION FUNCTION ANALYSIS.....	13
6. CONCLUSIONS	15
7. REFERENCES	16

LIST OF FIGURES

Figure 1. Schematic representation of the structure of (A) 14 Å tobermorite and (B and C) C-S-H with two different compositions (taken from [43]).....	3
Figure 2. (a) Custom tray for pellets, (b) resulting pellets after synthesis, and (c) sketch of the test specimens stacked in the irradiation and replica capsules [49].....	5
Figure 3. Monitored temperature during the irradiation experiment at three different locations.	6
Figure 4. Monitored temperature of the replica capsule at the same locations as those monitored for the irradiation capsule.	6
Figure 5. Duplicate capsule with samples exposed to same temperature profile as the irradiated samples.....	7
Figure 6. Samples in the capsules with custom tray in the middle (circled) for C-S-D pellets.	7
Figure 7. Thermogravimetry curves for control and irradiated C-S-D samples at Ca/Si ratio of 0.75 (left) and 1.33 (right).....	10
Figure 8. XRD patterns of the C-S-D control samples with bulk Ca/Si ratios of 0.75 (left) and 1.33 (right).	11
Figure 9. Irradiated sample preparation for XRD measurements.	11
Figure 10: XRD results for irradiated sample with Ca/Si ratio of 0.75.	11
Figure 11. XRD pattern comparison for pristine C-S-H sample with and without Kapton tape.	12
Figure 12. Neutron total scattering patterns of C-S-D gels with (a) Ca/Si of 0.75 and (b) Ca/Si of 1.33. The C-S-D samples were kept in the glovebox (black line), oven-dried (red dashed), and gamma- and neutron-irradiated (blue dotted). (c) and (d) show the pair distribution function of C-S-D gels with Ca/Si of 0.75 and 1.33, respectively.	14
Figure 13. D-O peak intensity (at ~0.95 Å) obtained from the neutron PDF data of C-S-D samples with different conditions.	15

LIST OF TABLES

Table 1. Weight percent associated with molecular water (H_2O^-), hydroxyl groups (H_2O^+), and total water content for control and irradiated samples.	10
Table 2. Basal spacing for the control samples.	12

ABBREVIATIONS

C-S-H	calcium silicate hydrate
C-S-D	calcium silicate deuterate
GGys	Gigagrays
LWRSP	Light Water Reactor Sustainability Program
MGys	Megagrays
NOMAD	Nanoscaled-Ordered Materials Diffractometer
ORNL	Oak Ridge National Laboratory
PDF	Pair distribution function
RH	relative humidity
SNS	Spallation Neutron Source
XRD	x-ray diffraction

ACKNOWLEDGMENTS

This research was sponsored by the US Department of Energy, Office of Nuclear Energy, Light Water Reactor Sustainability (LWRS) Program Materials Research Pathway under contract DE-AC05-00OR22725 with UT-Battelle LLC. The authors wish to thank Denise Adorno Lopes and Matt Kurley (senior R&D staff member and R&D Staff member respectively, Nuclear Fuel Cycle Division, Oak Ridge National Laboratory) for the assistance with thermogravimetry data collection, Michelle Everett for assistance with planning and performing the neutron pair distribution function (PDF) measurements at the Spallation Neutron Source (SNS), the Low Activated Materials Development and Analysis Laboratory (LAMDA) staff for assistance with sample preparation and transport to SNS, Thomas M. Rosseel for technical guidance, and Xiang (Frank) Chen, MRP Lead for his support for this research. The authors also wish to thank the US Nuclear Regulatory Commission for supporting the irradiation of the specimens at the LVR-15 test reactor in the Czech Republic. Technical staff at LVR-15 are acknowledged for performing the irradiation experiment and monitoring irradiation temperature.

EXECUTIVE SUMMARY

The US Department of Energy Office of Nuclear Energy Light Water Reactor Sustainability Program (LWRSP) has a research history of evaluating and predicting the effects of irradiation in the concrete biological shield that surrounds reactor pressure vessels. This program emerged in support of both the aging management and the license renewal of the US light-water reactor fleet up to 80 years of operation. The final goal of the Concrete Task in the Materials Research Pathway is to provide industry with tools to assess the expected damage in concrete biological shields at elevated irradiation doses that correspond to prolonged operation. This task requires the development of physics-based predictive models for damage and degradation of mechanical properties of concrete as a function of irradiation dose [1-4]. The development of these models has been a major activity within the Concrete Task.

The concrete biological shield is estimated to undergo levels of gamma and neutron irradiation on the order of 50–200 MGy [5-7] and 2×10^{19} – 7×10^{19} n/cm² ($E > 0.1$ MeV), respectively at 80 years of operation [8]. Concrete is composed of cement paste and aggregates. Aggregates are mainly affected by neutrons, which cause the aggregates to expand [4, 6, 9]. Cement paste, on the other hand, is mainly affected by gamma rays, which cause dehydration through hydrolysis [6]. The stresses caused by the expansion of the aggregates can be dissipated by two mechanisms: cracking [4] or relaxation within the cement paste. Understanding this stress relief is important because the viscous nature of the paste can be a factor in the mitigation of irradiation damage. Mechanical properties have been found to deteriorate after accelerated irradiation exposure of concretes and mortars [9]. The irradiation flux in test reactors, however, is two to three orders of magnitude higher than in commercial light-water reactors [8, 10], which could suggest that relaxation mechanisms can delay the onset of radiation damage [2, 3]. This delay has been predicted by a model that considers both creep (time-dependent deformation under constant load) and irradiation damage. In this model, creep was modeled to be independent of neutron fluence [2, 3]. However, considering a real case scenario with exposure to both neutrons and gamma rays, this assumption may not be correct because gamma rays can negatively affect the viscosity of the paste. Furthermore, some reported data on mechanical properties of mortar and concrete after gamma irradiation point toward a decrease of the creep response [11, 12]. The literature on this topic is very scarce and only considers relatively low gamma doses. Hence, higher doses, which are relevant to those estimated at prolonged operation, have been investigated in [13] and this report. Although the effects of neutrons on cement paste have been disregarded, molecular dynamics simulations of neutron bombardment in calcium silicate hydrates (C-S-Hs) have predicted a reorganization of its atomic structure. Simulated interatomic distances have shown increased disorder in irradiated C-S-H evidenced by broader peaks in partial pair distribution functions of the Si-O, Ca-O, Si-Si, Ca-Ca, O-O, and H-H bonds [14]. These reorganization and disorder of the atomic structure might impact the mechanical properties of these hydration phases. Neutron doses relevant to prolonged operation ($> 10^{19}$ n/cm²) are studied in this report.

Calcium silicate hydrates (C-S-Hs), also known as the glue of cement, are the strength-developing phases and occupy approximately 40% of the paste by volume. Most of the intrinsic viscoelastic behavior of the paste is attributed to these phases. C-S-Hs are, therefore, good analogues for cement paste. Creep in cement paste is explained by the sliding of particles, blocks, or sheets of C-S-H under sustained stress [15-18], although other mechanisms such as dissolution-precipitation of hydrates (both C-S-H and calcium hydroxide) have been discussed in literature [19-21]. The stress relaxation of C-S-H is heavily dependent on its water content [15]. Other studies report a dependence on its chemical composition and structure: mean silicate chain length or degree of cross-linking (chain-branching silicate sites) [22].

In this study, compressed pellets of calcium silicate deuterate (C-S-D) with bulk Ca/Si ratios of 0.75 and 1.33 were irradiated in an out-of-core position at the LVR-15 reactor at Centrum vyzkumu ReŽ in the Czech Republic to an estimated neutron and gamma irradiation absorbed doses of 1.22×10^{19} n/cm² ($E > 0.1$ MeV)

and 1.02 GGy, respectively. Doses were obtained from Monte Carlo N-particles simulations and the activations of metals coupons placed in the irradiation capsule. Control specimens were exposed to the same temperature history as the irradiated samples; additionally, a set was stored in a moisture- and inert gas-controlled glove box at approximately 11% relative humidity. The samples were synthesized with deuterium to improve contrast for neutron pair distribution function (PDF) experiments. H has a large neutron cross-section and signal coming from H dominates most of the scattering, therefore it is always preferable to avoid H content in samples when performing this kind of measurement.

Thermogravimetric analysis was used to determine the total water content, X-ray diffraction (XRD) measurements were used to calculate the dimension of the basal spacing that is related to the interlayer water, and neutron total scattering and pair distribution function analysis were performed on the Nanoscaled-Ordered Materials Diffractometer (NOMAD) instrument at the Spallation Neutron Source (SNS) at Oak Ridge National Laboratory to investigate the interatomic distances in the structure. X-ray diffraction and thermogravimetry both showed that the control samples for Ca/Si ratio of 0.75 showed minimal differences in water content, suggesting that the thermal effect is negligible for this Ca/Si ratio. However, thermogravimetry showed that irradiation did promote the loss of further water in the structure for this composition. For Ca/Si ratio of 1.33 the comparison between the heated control sample and the irradiated sample in terms of thermogravimetry results showed minimal change in water content, suggesting that thermal and irradiation effects were on the same order for this composition. Thermogravimetry and neutron scattering experiments revealed that the sample with Ca/Si ratio of 0.75 was more affected by irradiation than that of Ca/Si of 1.33. Neutron scattering experiments showed water loss with heating and further water loss with irradiation, evidenced by the decrease in intensity of the D-O peak. However, this effect was less pronounced for the sample with Ca/Si ratio of 1.33. Additionally, depolymerization was observed with heating and irradiation, suggested by the decrease of the Si-Si correlation peak intensity. The fact that the sample with high Ca/Si ratio is less affected by irradiation can have implications on the design of concrete structures for nuclear power plants, since blended cementitious systems that promote high Ca/Si ratios in C-S-H would be more irradiation resistant.

1. INTRODUCTION

1.1 MOTIVATION OF THE STUDY

This work is part of the Materials Research Pathway of the LWRSP to support the license renewal of selected light-water reactors in the US fleet for an extension to up to 80 years of operation and beyond. Such extension would result in the concrete biological shield to be exposed to estimated neutron and gamma doses of $2 \times 10^{19} - 7 \times 10^{19}$ n/cm² ($E > 0.1$ MeV) [8] and 50–200 MGy [5-7], respectively.

A major focus within the LWRSP has been the development of physics-based predictive models of irradiation damage in concrete [1, 3, 4]. An extensive literature review on the effects of irradiation in concrete, mortars, and cement concluded that neutrons cause expansion of minerals present in aggregates (radiation-induced volumetric expansion) [9], and that cement paste suffers dehydration through hydrolysis due to exposure to gamma rays [6]. Concrete typically can dissipate stresses caused by the expansion of the aggregates via two mechanisms: cracking or relaxation. Creep (time-dependent deformation under constant load) delays the onset of predicted irradiation damage in concrete [3]. This delay indicates that the viscous nature of cement paste plays a role in the mitigation of irradiation damage. In the predictive model detailed in [3], creep was assumed to be independent of fluence, and neutrons were the only source of radiation that was considered. However, light-water reactor's concrete biological shield is exposed to both neutrons and gamma rays. Thus, the viscous response of the cement paste may be altered by the dehydration through hydrolysis [23]. Limited literature exists on gamma-irradiated cementitious systems; however, the very few available studies indicate a reduction of the creep rate with increasing radiation exposure [11, 12]. This creep rate reduction needs further investigation and validation. A decrease in viscous behavior would hinder the ability of the paste to relax stresses, which will affect the predicted irradiation damage suggesting that it may be underestimated in predictive models.

C-S-H occupies about 40% in volume of the hydrated cement paste and is responsible for the strength and viscous behavior of the paste. This makes C-S-H a good cement paste analogue. The effects of a gamma irradiation dose up to 189 MGy on mechanical and chemical-structural properties of C-S-H were reported previously [13, 24-28]. The gamma irradiation dose that a concrete biological shield in a nuclear power plant endures during an 80-year design life is approximately 100–200 MGy. However, precise changes in the mechanical properties and atomic environments of C-S-H at ultrahigh irradiation dosages have only been recently documented. Baral et al. [13] reported that irradiation decreased the C-S-H basal spacing and increased its Young's modulus due to a densification of its structure. Irradiation also decreased the molecular water content and increased hydroxyl groups in C-S-H, effectively showing that interlayer water removal reduced the basal spacing. Additionally, ¹H and ²⁹Si nuclear magnetic resonance results indicate some disorder in the local proton CaO–H species and slight depolymerization of the silicate structure. Together, these results indicate that the C-S-H gel stiffens upon ultrahigh gamma irradiation dosage.

The effects of neutrons on cement paste have seldomly been researched. However, theoretical studies suggest an atomic reorganization of C-S-H upon neutron bombardment, causing broadening of the partial pair distribution functions (PDFs) [14]. Interestingly, the effects of neutron bombardment were found to be dependent on Ca/Si ratio, suggesting that low Ca/Si was more affected by irradiation. A Ca/Si of 1.5 presented the less irradiation damage. Neutron PDF has also been employed to follow how dehydration affects the structure of C-S-D [29]. Deuterium was chosen instead of H because H has a large neutron cross-section and can yield undesirable backgrounds in neutron experiments. Given how both neutron and gamma can have effects in the atomic structure of C-S-H, PDF is a very good tool to study the effects of both types of radiation on cement hydrates.

For this report, synthetic calcium silicate deuterate (C-S-D) with Ca/Si ratios of 0.75 and 1.33 were exposed to neutron and gamma irradiation absorbed doses of 1.22×10^{19} n/cm² ($E > 0.1$ MeV) and 1.02 GGy,

respectively. Their properties were compared with those of control specimens. The control specimens were exposed to the same temperature history as the irradiated samples; additionally, a set was stored in a moisture- and inert gas-controlled glove box at approximately 11% relative humidity (RH).

Thermogravimetric analysis was used to determine the water content, and X-ray diffraction (XRD) measurements were used to calculate the dimension of the basal spacing that is related to the interlayer of water. Neutron pair distribution function analysis measurements were taken on the NOMAD instrument at the Spallation Neutron Source (SNS) at Oak Ridge National Laboratory (ORNL) to investigate the interatomic distances in the structure. Nanoindentation will be performed in the future to investigate mechanical properties.

1.2 EFFECTS OF GAMMA RAYS AND NEUTRONS ON CEMENT AND CEMENT HYDRATES

This section was partly discussed in previous milestone reports [24, 25, 28] and has been modified in this report.

Previous studies have detected H release during gamma irradiation of cement pastes pre dried to 120°C, suggesting that gamma rays can decompose chemically bound water in cement hydrates [6], although to a low extent (~1.5% at 200 MGy). Hydration products and anhydrous cement grains were shown to decompose at gamma doses <130 MGy [30]. This decomposition causes the appearance of pseudomorphoses because of the loss of chemically bound water. Microcracking and a densification of the hydration shell have also been observed at gamma doses of <290 MGy [30]. The presence of certain ions in the pore solution can affect the H release through hydrolysis. Studies have shown that adding NaNO₃ to ordinary Portland cement almost suppresses the H production [31], and the addition of FeOOH to tricalcium silicate pastes, with Fe mostly present in the pore solution, increases the H release [32]. Regarding adsorbed water, the H release from hydrolysis depends on the nature of the substrate [33]. The confinement of water in the nanopores of controlled pore glass materials and mesoporous silica yields a H release larger than that of free water. In the case of the glass materials, the ionizing energy is deposited in the silica and is almost completely transferred to the confined water, causing direct hydrolysis [34]. The complexity of both the radiolysis chemistry and the nature of cement as a substrate are direct causes for the poor understanding of the effects of gamma irradiation on cementitious materials. Specifically, the radiochemistry is very complex [35]; the structures of the hydrates, such as C-S-H, are complex. C-S-H is a layered material with a defective tobermorite-like structure; and the different water populations present in the system (ion-charged capillary, adsorbed and chemically bonded water) can experience varied radiolysis rates depending on their chemical surroundings and nature.

The effects of gamma rays on cement hydrates (C-S-H) have been extensively investigated within the LWRS program. Doses from approximately 1MGy to 189 MGy have been studied [13, 26, 27]. Doses up to 2 MGy have shown to have no effect on chemical-structural and mechanical properties [26, 27], while doses of 25 MGy and 189 MGy affect the structure of the hydrates by decreasing the interlayer water and in consequence the basal spacing [13]. This yields a densification of the structure that promotes stiffening, an increase in Young's modulus and a decrease in creep. Additionally, gamma irradiation promotes the formation of hydroxyl bonds.

The effect of neutrons on cement hydrates has been vaguely investigated and only theoretical studies can be found in the literature [14]. Simulations of neutron bombardment in C-S-H with molecular dynamics have shown that irradiation influences the structural order, silicate mean chain length, and molecular water content. C-S-H was found to be more radiation resistant at high Ca/Si of 1.5. C-S-H compositions that are more rigid and stressed (Ca/Si < 1.5) exhibit large changes with irradiation, however those compositions that are associated to more flexible structures (Ca/Si = 1.5) show less variations in their atomic structure

[14]. Supporting documentation for this study also includes simulated partial pair distribution functions that show peak broadening with irradiation. This is attributed to the atomic disorder induced by neutron bombardment.

1.3 STRUCTURE AND MECHANICAL PROPERTIES OF C-S-H

This section was already discussed in previous milestone reports [24, 25, 28] and has been slightly modified in this report.

C-S-H forms by the hydration of both tricalcium and dicalcium silicate, it is the strength-developing phase and occupies more than 40% of the volume of hydrated cement. Its structure is similar to that of the natural mineral tobermorite. C-S-H has central complex layers of calcium and oxygen atoms sandwiched by dreierketten-type silicate chains (see Figure 1). These layers are stacked with chemically bound water in the interlayer space [36, 37]. C-S-H also contains gel water, which is in the nano porosity that is thought to be the result of the random arrangement of sheets during the growth of C-S-H [23, 38-40].

In pure ordinary Portland cement, C-S-H has an average Ca/Si ratio of approximately 1.75 [41], but in blended systems, the composition of C-S-H varies extensively (Ca/Si ratio from 0.7 to 2.1) [42]. The mean silicate chain length and the interlayer- or basal spacing- of C-S-H decrease with increasing Ca/Si ratio. There are two mechanisms that could potentially explain this decrease: one is the removal of the bridging tetrahedra and the inclusion of Ca^{2+} ions in the interlayer [43] (see Figure 1). The other mechanism implies an interstratification of layers of tobermorite dimers and tobermorite infinite layers with an increasing number of tobermorite dimers as the Ca/Si ratio increases [44]. In cementitious systems with Al^{3+} available to react, a fraction of the bridging tetrahedra are substituted by Al^{3+} , giving rise to Al-substituted C-S-H or C-A-S-H [45].

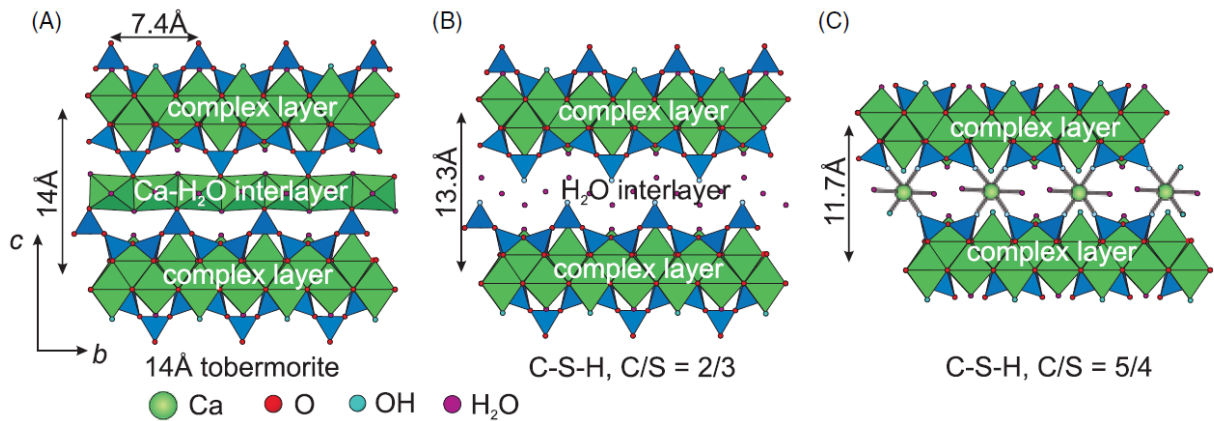


Figure 1. Schematic representation of the structure of (A) 14 Å tobermorite and (B and C) C-S-H with two different compositions (taken from [43]).

The amplitudes and rate of creep in C-S-H are larger than those from the other hydration phases. The mechanisms that influence creep in C-S-H are still under debate, but the most agreed upon mechanism is the viscoelastic sliding of particles, blocks, or sheets with respect to each other [15-18]. A stress-induced dissolution-precipitation mechanism has also been presented in literature [19-21]. A recent model of the growth of C-S-H considers a specific type of bond between C-S-H sheets that comprises Ca ions bridging between O atoms in silicate groups [46]. These bonds that bridge O and silicate groups could potentially move from one site to an adjacent one due to stress and thermal activation, which could be the origin of creep in C-S-H.

The stress relaxation of C-S-H depends on its water content: saturated specimens exhibit a hydrodynamic component corresponding to pore water, whereas specimens dried to 11% RH and further do not, and their viscous response is an effect of deformations of the solid body [15]. The partial removal of interlayer water also lowers the stress relaxation in C-S-H [15]. The interlayer water has a more significant structural role for high Ca/Si C-S-H because the viscous response is more easily affected by drying to 11% or lower RH than for low Ca/Si C-S-H [15]. Some researchers have found that the viscous response of C-S-H is also dependent on the chemical structure and elastic properties [15, 22, 47]. One hypothesis is that a higher Ca/Si ratio and associated decrease in both mean aluminosilicate chain length and degree of cross-linking (Q^3) lead to a larger amount of sliding blocks per gram of material that would exhibit a more viscous response—for instance, tricalcium silicate pastes cured at high temperatures (more polymerized than at low temperatures) show less creep [48]. The Al-substituted C-(A)-S-H was also found to be less viscous than C-S-H given its longer aluminosilicate chain length and the presence of cross-linking, which were thought to offer more resistance to the sliding of particles under load [22].

2. SAMPLE SYNTHESIS

Heavy water was used in the synthesis to avoid the presence of H in the samples so that neutron scattering PDF experiments could be performed without the signal being dominated by H. C-S-D was synthesized by mixing freshly produced CaO (by calcining CaCO_3 at $1,000^\circ\text{C}$ overnight) and nano silica. Heavy water was used with a water-to-solid ratio of 16. The Ca/Si ratios of 0.75 and 1.33 were targeted in the synthesis. The powders and the heavy water were mixed in a high-density polyethylene bottle that was sealed in an inert gas atmosphere. Milling balls were also introduced in the bottle as milling media. The samples were then taken out of the glove box to mill the mixtures in a roller mill for 3 days. After milling, the bottles were taken back to the glove box, where the slurries were extracted from the bottles in an inert atmosphere to prevent carbonation, and they were filtered in a Buchner funnel with P4 filter paper. They were then dried at 60°C with a N_2 flow of $50 \text{ cm}^3/\text{min}$ for 4 days. After drying, the resulting blocks of material were crushed in a mortar and pestle and passed through a $75 \mu\text{m}$ sieve inside the glove box. The sieved powders were conditioned to 11% RH in sealed containers with the use of saturated LiCl solutions. Carbonation was also prevented by placing granular soda lime in the sealed containers. The powders were compressed in pellets using a hydraulic press at 250 kN and 0.17g of sample were used for each pellet. The resulting dimensions of the pellets were approximately 10 mm in diameter and 2 mm thick (see Figure 2). They were stored in the containers at 11% RH before the irradiation was performed.

3. IRRADIATION DETAILS

The irradiation conditions were accelerated in a test reactor to achieve an irradiation-to-fluence level $>10^{19} \text{ n/cm}^2$ at $E > 0.1 \text{ MeV}$ in a timely manner. Although several test reactors are available around the world, the irradiation conditions and test setup must meet several criteria to ensure that the effects of irradiation-induced temperature do not impair the interpretation of the test data. Because the irradiation temperature inside concrete is governed by the energy deposition caused by thermal neutrons and gamma-induced heating, the number of test reactors of interest is limited. After completing a survey of the test reactors, the LVR-15 reactor at Centrum vyzkumu Rež in the Czech Republic was selected as the best option for this experiment. The target fluence was $>10^{19} \text{ n/cm}^2$ ($E > 0.1 \text{ MeV}$). The gamma dose rate profile exhibits a parabolic trend with a maximum value of 34 Gy/s at mid height and $\approx 25 \text{ Gy/s}$ at the lower and higher extremities [49]. Two pellets of each Ca/Si ratio were placed in a custom alumina tray and introduced in a custom Al capsule together with concrete cores with and without reinforcement (see Figure 2). A flow of 0.05 l/min of He gas was continuously purging the capsule while irradiation took place. The experiment was completed in 14 irradiation cycles over approximately 2 years. Temperature cycle profiles were recorded over the course of the experiment in three different locations (see Figure 3) with k type thermocouples. CVR provided the temperature profiles of each irradiation cycle and those were matched in

an oven for one of the control sets (see Figure 4). A duplicate capsule with the same concrete specimens and C-S-D pellets was subjected to those temperature profiles for the 2 years of the experiment (see Figure 5 and Figure 6).

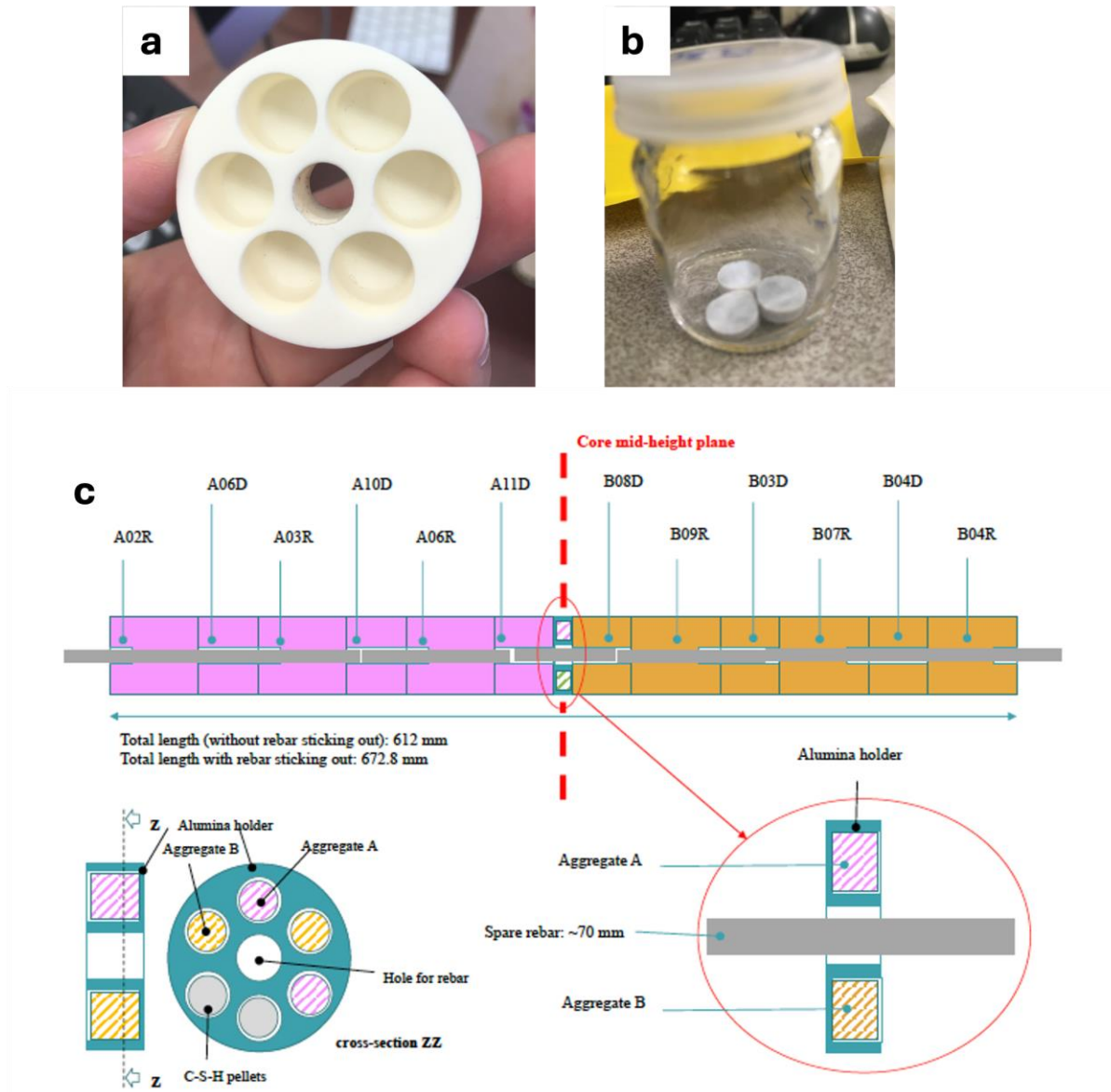


Figure 2. (a) Custom tray for pellets, (b) resulting pellets after synthesis, and (c) sketch of the test specimens stacked in the irradiation and replica capsules [49].

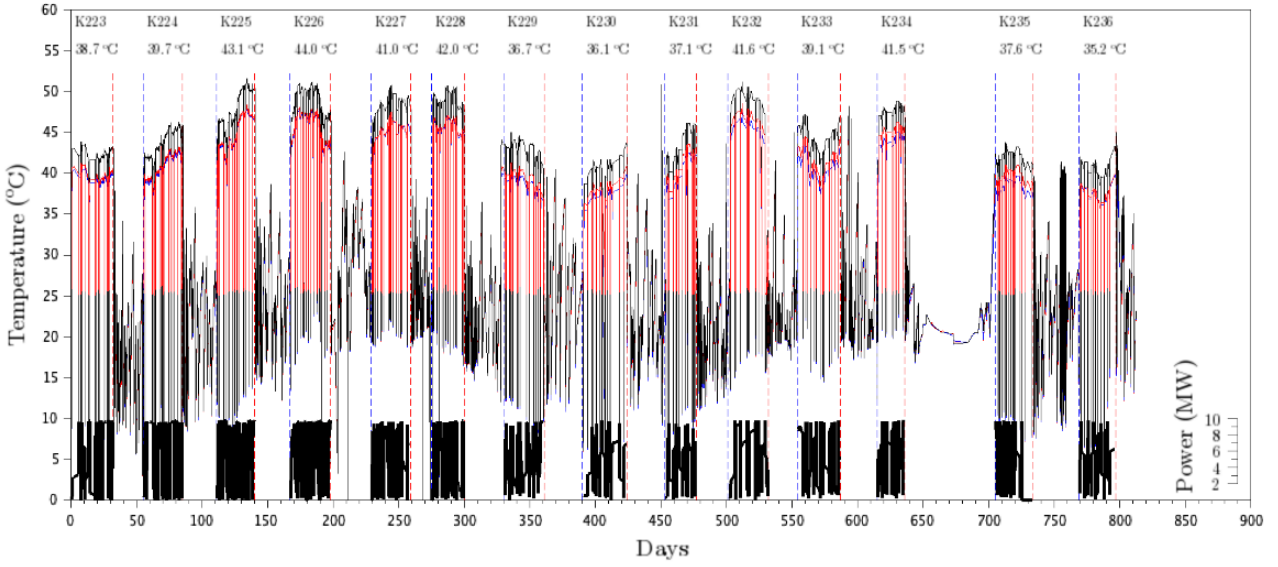


Figure 3. Monitored temperature during the irradiation experiment at three different locations.

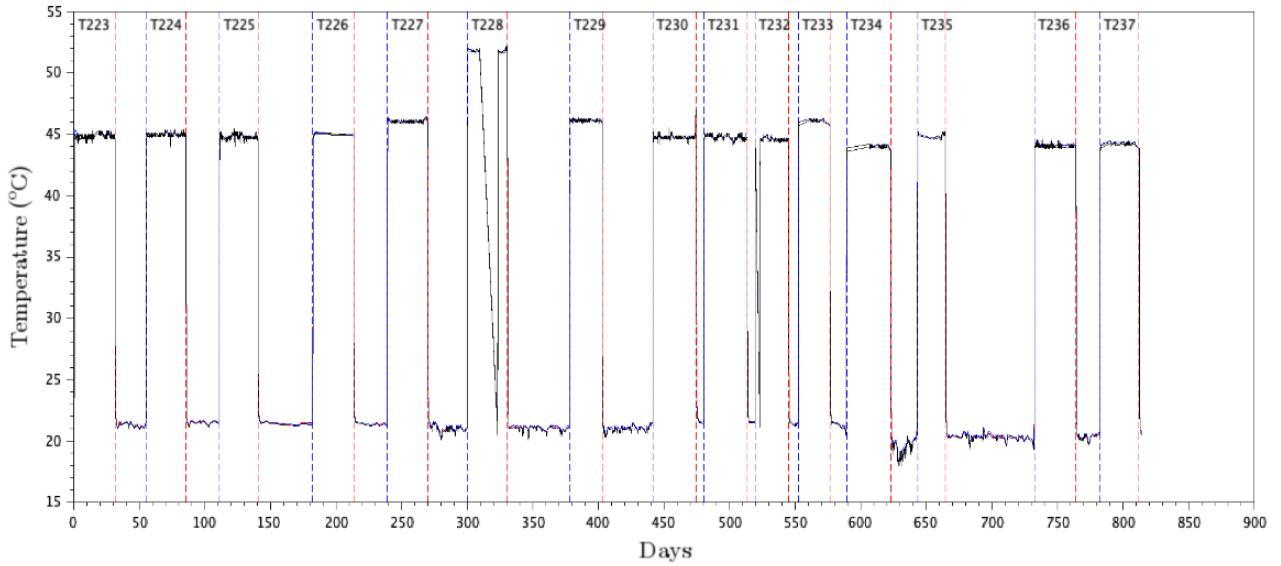


Figure 4. Monitored temperature of the replica capsule at the same locations as those monitored for the irradiation capsule.



Figure 5. Duplicate capsule with samples exposed to same temperature profile as the irradiated samples.



Figure 6. Samples in the capsules with custom tray in the middle (circled) for C-S-D pellets.

4. EXPERIMENTAL DETAILS FOR POSTIRRADIATION EXAMINATION

The control specimens mentioned in this section were pellets that were preconditioned to 11% RH and kept in a glovebox purged with He at this relative humidity. Another batch of control pellets were in an oven under the same temperature conditions as the irradiated ones. Both sets of control pellets were made from the same batch of synthesized material than their respective irradiated samples.

4.1 THERMAL ANALYSIS

Thermogravimetric analysis was performed in an STA 449 F3 Jupiter equipped with Netzsch Proteus 8.0.3 software. A portion of the pellets was ground in an agate mortar and pestle. For the analysis, approximately 15 mg of each sample were used. The samples were heated from 20°C to 1,000°C at a rate of 20°C/min, monitoring their weight loss. During analysis, an Ar flow of 50 mL/min was used while heating.

4.2 X-RAY DIFFRACTION

Diffraction patterns of the samples were acquired with a D2 PHASER desktop X-ray diffractometer that operates at 30 kV and 10 mA. Data were acquired for 2θ from 5° to 80° , a step size of 0.03° , and a time per step of 3 s. For basal spacing calculation, the profile fitting option of HighScore Plus [50] was used. The peaks were fitted using a Pseudo Voigt function, split width for asymmetry, and peak base width of 45° while keeping the background determined in the previous step unchanged. In total, 10 peaks with 2θ values around 8.4° , 16.2° , 27.6° , 29.2° , 31.9° , 42.8° , 50.0° , 55.0° , 61° , and 66° were chosen to be the starting points of the profile fitting. The profile fitting function was run until a minimum in least square residuals was found. Typically, a minimum was found within less than 40 cycles. The goodness of fit was 1.2–1.8, and the R_{wp} (weighted $R_{profile}$) was 2.3–3.5 for all fittings. No internal standard was used, so the fitted profile of the irradiated samples was shifted such that the main peak at around 29.2° 2θ overlapped with the glove box control samples of same Ca/Si to correct for any sample surface displacement. This peak is the most intense reflection for C-S-H, and its shift can be considered negligible for the reached temperatures [51]. The basal spacing d was calculated by applying the diffraction condition equation (Equation 1) using the position of the shifted basal reflection (lowest angle at which there is a peak):

$$n\lambda = 2d \sin \theta, \quad (1)$$

where λ is the wavelength of the X-ray source (for a $\text{CuK}\alpha$, $\lambda = 1.54056 \text{ \AA}$), θ is half of the incident angle at the position of the desired peak, and in this case, the integer $n = 1$. The errors in the peak positions given by the fittings were used to calculate the errors for the basal spacing.

An attempt to study the irradiated samples was done by covering the packed powder with kapton tape. This is a usual procedure to analyze radioactive materials such as uranium nuclear fuel related samples. Kapton tape is used to prevent contamination of the instrument. Furthermore, it is a very common material used with hazardous samples under X-ray examination because it has a desirable low background.

4.3 NEUTRON PAIR DISTRIBUTION FUNCTION ANALYSIS

Total scattering and pair distribution function (PDF) analysis are important methods for investigating the crystalline structure and atomic-scale arrangement of materials [52]. By Fourier transforming neutron or synchrotron-based X-ray total scattering data, PDF elucidates the probability of finding two atoms at specific distances. Thus, PDF analysis is valuable for resolving the local atomic environment in non-crystalline structures. This technique is crucial for studying cementitious systems, where the final gel products are typically amorphous or nano-crystalline. Previous studies have successfully adapted the PDF analysis to elucidate the various atomic-scale properties of the cementitious systems including carbonation [53], dehydration [29], retardation [54], and reaction kinetics [55, 56].

Neutron PDF measurements were performed at the Nanoscaled-ordered materials diffractometer (NOMAD) beamline at the Spallation Neutron Source (SNS) at ORNL. The instrument is a high-flux, medium-resolution diffractometer with a large bandwidth of neutron energies and extensive detector coverage to perform structural determinations of local order in crystalline and amorphous samples. Its capabilities allow for the studies of a large variety of materials ranging from liquids, solutions, glasses, polymers, nanocrystalline samples to long-range-ordered crystals. The enhanced neutron flux at SNS, coupled with advanced neutron optics and detector features of NOMAD, allow for access to high-resolution pair distribution functions.

The C-S-D samples were introduced in thin glass capillaries under a He atmosphere in a glovebox. The capillaries were sealed with epoxy. The gas environment was chosen to suppress the presence of air, and the gases that conform it, such as N and water vapor, that can result in undesirable background for the

experiments. Data sets were collected at room temperature. To obtain the total scattering functions and resulting PDFs, the data sets were normalized by the scattering of a vanadium rod and the background of an empty glass capillary was subtracted.

The PDF, $G(r)$, was calculated by a Fourier Transform of the total scattering function, $S(Q)$:

$$G(r) = \frac{2}{\pi} \int_{Q_{min}}^{Q_{max}} Q[S(Q) - 1] \sin(Qr) dQ , \quad (2)$$

Where $Q = 4\pi \sin\theta / \lambda$, and $Q_{max} = 20 \text{ \AA}^{-1}$.

5. RESULTS AND DISCUSSION

5.1 THERMAL ANALYSIS

The weight loss curves for control and irradiated samples are shown in Figure 7. The curves show the typical dehydration of C-S-H, with most of the weight loss occurring before reaching 200°C [51, 57]. The control samples seem to be pure because the dehydration of Ca(OH)_2 (at ~400°C) and decarbonation of carbonates (at ~600°C) [36] steps are not observed. However, the irradiated samples exhibit a weight loss step around ~600°C that is attributed to carbonates. The irradiated samples and the control samples from the oven were conditioned under an inert gas flow, and while the samples from the oven do not exhibit the weight loss typical from carbonates, irradiation seemed to have promoted carbonation. This agrees with other observations of carbonation eased by radiation environments [58, 59], although it is surprising that under an inert gas flow carbonation still occurred in this experiment. The total loss at 1,000°C was taken as the total water weight percentage.

In reviewing the literature, various approaches are used to relate the thermogravimetric mass loss of C-S-H in several temperature intervals to molecular water and hydroxyl groups. Cong and Kirkpatrick [60] assumed the mass loss up to 110°C corresponded to molecular water, whereas the mass loss from 110°C to 1,000°C corresponded to the release of -OH groups. Garbev et al. [57] did not investigate the molecular water content but assigned the mass loss mostly to Si-OH groups from 770°C to 900°C when increasing the temperature at 10°C/min. Roosz et al. [61] took the mass loss at 150°C to be the total molecular water content and assigned the mass loss from 150°C to 700°C as dehydroxylation. Yin et al. [62] assigned the mass loss up to 300°C as the molecular water content. Hunnicutt [63] analyzed Al-substituted C-S-H phases using a heating rate of 10°C/min and assigned the mass loss from 25°C to 180°C as surface water, 180°C to 370°C as dehydration of C-S-H and removal of adsorbed water, 395°C to 565°C as dehydroxylation, and 550°C to 1,000°C as the transformation to beta-wollastonite and mayenite.

For the analysis presented here, the weight loss between 20°C and 400°C was assigned to molecular water (free and interlayer), and the weight loss between 400°C and 1,000°C was associated with the release of hydroxyl groups and the transformation to beta-wollastonite. The partial weight losses and the total water content are included in

Table 1. The control samples with a Ca/Si ratio of 0.75 have very similar total water contents, indicating that the heating treatment did not remove any extra water. The irradiated sample with Ca/Si ratio of 0.75 lost more total water content during irradiation, which aligns with the findings in Baral et al [13]. On the other hand, the control samples with Ca/Si ratio of 1.33 seem to be affected by the conditioning; the sample in the glove box contains less water than the one kept in the oven. As can be seen in Figure 7 (right), the measurement for the control sample kept in the oven exhibits an abnormally high buoyancy effect. This

effect can be corrected with a baseline that is obtained by running the same program with an empty crucible and the examination of this sample will be repeated to account for this correction. But if the irradiated sample is compared to the control sample kept in the oven, there is not a significant difference in the total water content of both materials.

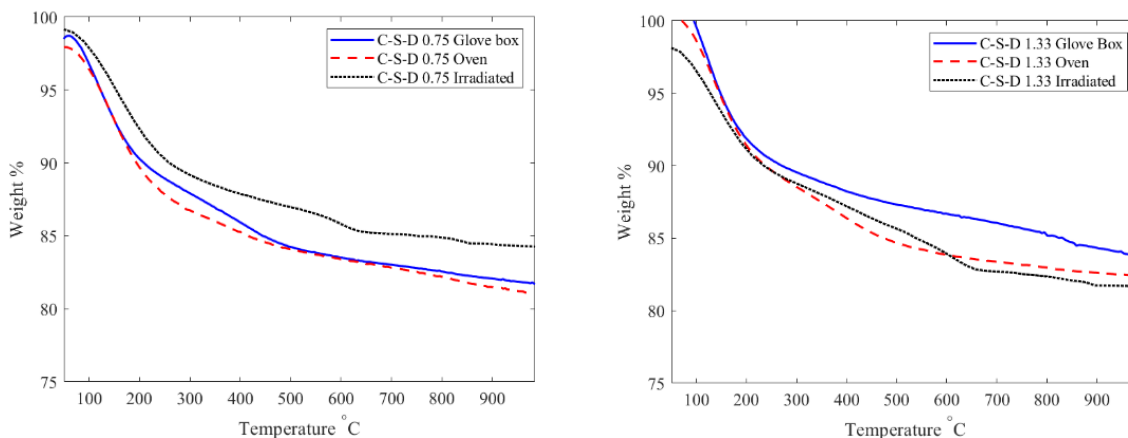


Figure 7. Thermogravimetry curves for control and irradiated C-S-D samples at Ca/Si ratio of 0.75 (left) and 1.33 (right).

Table 1. Weight percent associated with molecular water (H_2O^-), hydroxyl groups (H_2O^+), and total water content for control and irradiated samples.

Bulk Ca/Si ratio		H_2O^- (wt %)	H_2O^+ (wt %)	Total H_2O (wt %)
0.75	Glove box	12.37	5.31	17.68
	Oven	11.90	5.50	17.40
	Irradiated	12.12	3.92	16.04
1.33	Glove box	11.79	5.10	16.89
	Oven	13.70	4.84	18.54
	Irradiated	12.82	5.91	18.73

5.2 X-RAY DIFFRACTION

The XRD patterns for control samples are shown in Figure 8. Comparing the intensities of the patterns of both control samples for each Ca/Si ratio it can be seen that the samples kept in the oven suffer a decrease in intensity for the overall pattern due to disordering of the structure. The samples with Ca/Si ratio of 0.75 clearly show that the basal distance (calculated from the first peak as explained in Equation 1) does not significantly change, as can also be seen in Table 2, but the intensity at that angle is distinctly attenuated.

The same effect can be seen in the control samples with Ca/Si of 1.33 with the significant difference that the angle is indeed shifted for the basal reflection between the two controls.

The irradiated samples were prepared according to the safety protocols for radiological materials, which suggest covering the samples with Kapton, as shown in



Figure 9 (right). The pattern for the irradiated sample of Ca/Si of 0.75 showed humps covering most of the peaks of interest (Figure 10). A test was conducted with a pristine C-S-H sample to compare the XRD patterns of holders mounted with and without kapton and determine if the humps were indeed due to irradiation or a result of the sample preparation. As shown in Figure 11, the background was indeed introduced by the Kapton. Therefore, it was decided to resort to the use a beamline either at the Spallation Neutron Source at ORNL or at a synchrotron user facility to measure the irradiated samples. An X-ray synchrotron source is more powerful than a benchtop diffractometer, which should help to resolve the peaks. Neutrons will also penetrate through a Kapton's protective layer and might be a better option than a conventional benchtop X-ray diffractometer. Consequently, no XRD data for irradiated samples will be presented in this report.

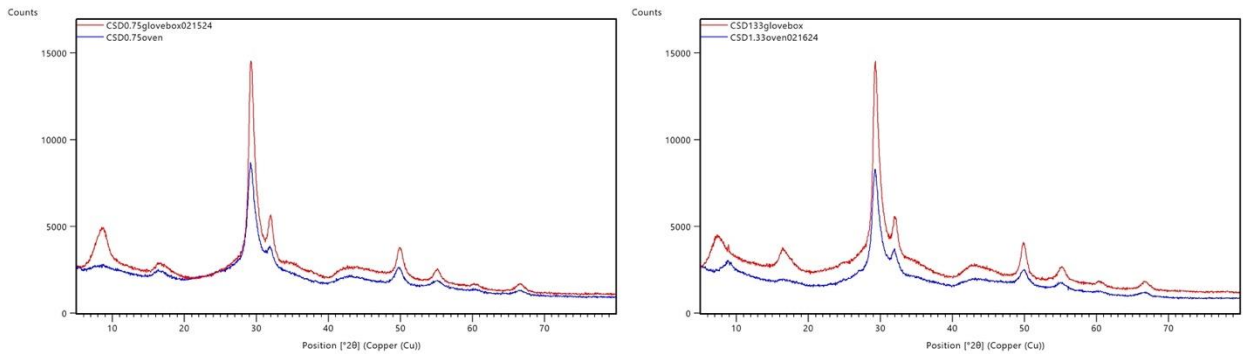


Figure 8. XRD patterns of the C-S-D control samples with bulk Ca/Si ratios of 0.75 (left) and 1.33 (right).



Figure 9. Irradiated sample preparation for XRD measurements.

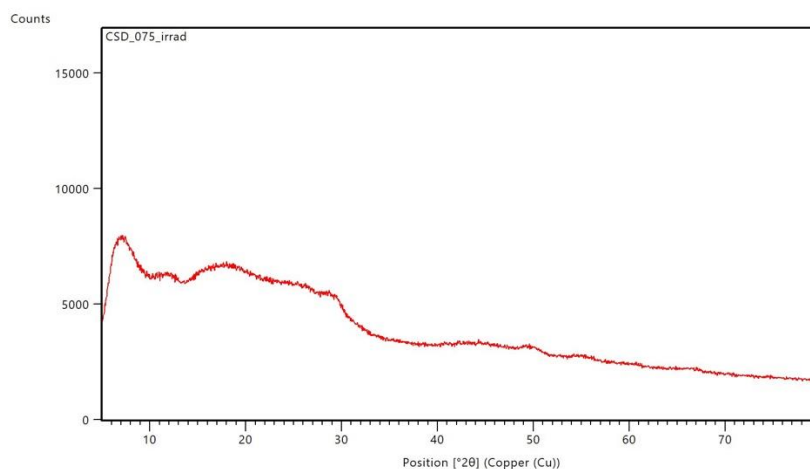


Figure 10: XRD results for irradiated sample with Ca/Si ratio of 0.75.

To obtain the position of the basal spacing, profile fitting was done in HighScore Plus [50] using the same procedure described in previous examinations [13, 28]. The basal distances that were calculated from the profile fittings are listed in

Table 2. The difference in the basal spacings for both control samples of Ca/Si ratio of 0.75 was negligible, which correlates with the TG findings of similar total water content, indicating that the thermal treatment in the oven did not promote further water loss than the preconditioning of the samples. The shift of the basal distance between the control samples with a Ca/Si ratio of 1.33 indicate the loss of interlayer water with the heating treatment. This approximately 20% difference occurs even though the samples were subjected to a maximum temperature of only roughly 40°C to 45°C. The results for Ca/Si ratio of 1.33 do not correlate with the TG observations, since the glovebox sample shows a higher basal spacing and that should translate into larger water content. Since this sample showed anomalous buoyancy in the TG measurements, the XRD findings stress the importance of repeating the TG measurement.

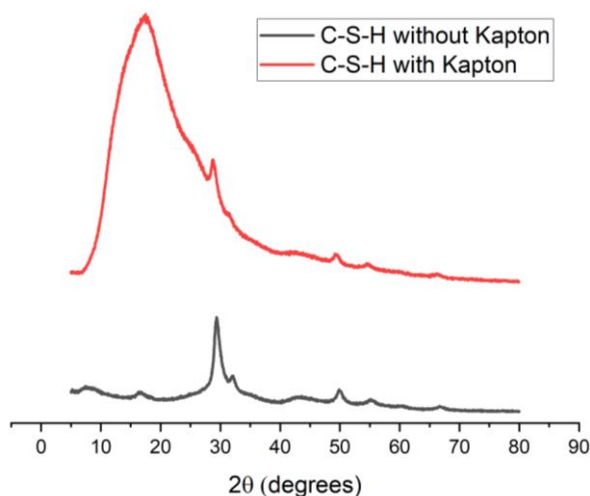


Figure 11. XRD pattern comparison for pristine C-S-H sample with and without Kapton tape.

Table 2. Basal spacing for the control samples.

Bulk Ca/Si ratio	Sample	Basal spacing (Å)
0.75	Glove box	10.55 ± 0.01
	Oven	10.39 ± 0.01
1.33	Glove box	12.34 ± 0.04
	Oven	10.03 ± 0.04

5.3 NEUTRON PAIR DISTRIBUTION FUNCTION ANALYSIS

The effects of oven-drying and gamma- and neutron-irradiation on C-S-D were investigated using neutron total scattering and PDF analysis. Figure 12 (a, b) displays the neutron reciprocal space structure factor of C-S-D with Ca/Si ratios of 0.75 and 1.33. For C-S-D with a Ca/Si ratio of 0.75 (Figure 12 a), the broad diffuse peak between Q values from 1 to 3.5 \AA^{-1} decreased after oven-drying, indicating water removal from the C-S-D gel structure [29, 64]. This diffuse peak further decreased in the irradiated C-S-D specimen. For the Ca/Si ratio of 1.33 (Figure 12b), the hump between Q values from 1 to 3.5 \AA^{-1} also decreased in the irradiated specimen; however, the change was less significant compared to the Ca/Si ratio of 0.75. This correlates with the TG findings that supported a larger effect on water loss due to irradiation for the sample with Ca/Si ratio of 0.75.

Figure 12 (c, d) presents the neutron PDF analysis for C-S-D gels with Ca/Si ratios of 0.75 and 1.33. The local atomic structure of the C-S-D samples showed the atom-atom correlations of D-O, Si-O, Ca-O, O-O, and Si-Si, which were assigned based on previous literature [29, 53]. The peak at approximately 0.95 \AA ,

indicating the D-O atom-atom correlation, provides further evidence of water removal induced by oven drying and irradiation. For both Ca/Si 0.75 and 1.33 C-S-D samples, the D-O peak decreased with oven-drying and further decreased with gamma- and neutron-irradiation, indicating water loss due to hydrolysis. Similar to the neutron diffraction patterns (Figs. 1a and 1b), the change in the D-O peak was less prominent for the Ca/Si ratio of 1.33, as shown in Figure 13. Other water-related correlations (D-O and D-D), positioned between 3 and 4.5 Å, also decreased with oven-drying and irradiation. Conversely, the intensity of the Si-O, Ca-O, and O-O correlations increased with oven-drying and irradiation. This increase is attributed to the reduction in atomic number density (ρ_0) due to the water removal from the C-S-D gel structures [29].

The neutron total scattering and PDF analysis results consistently show water loss from C-S-D gel structures with oven drying, and more intensive water removal upon gamma- and neutron-irradiation exposure. Moreover, the effect of oven-drying and irradiation was less significant in the higher Ca/Si C-S-D samples (Ca/Si = 1.33). Krishnan et al. [14] investigated the impact of irradiation on the structure of C-S-H using molecular dynamics simulations. They reported that C-S-H with a higher Ca/Si ratio has more resistance to irradiation compared to C-S-H with a lower Ca/Si ratio, which aligns with our results. Additionally, they suggested that the mean chain length of the C-S-H decreased with irradiation due to the depolymerization of the silicate chain. The depolymerization of the silicate chain in the gel structure upon irradiation was also observed in our research; the Si-Si correlation at ~ 3.1 Å decreased with irradiation exposure for both Ca/Si C-S-D samples.

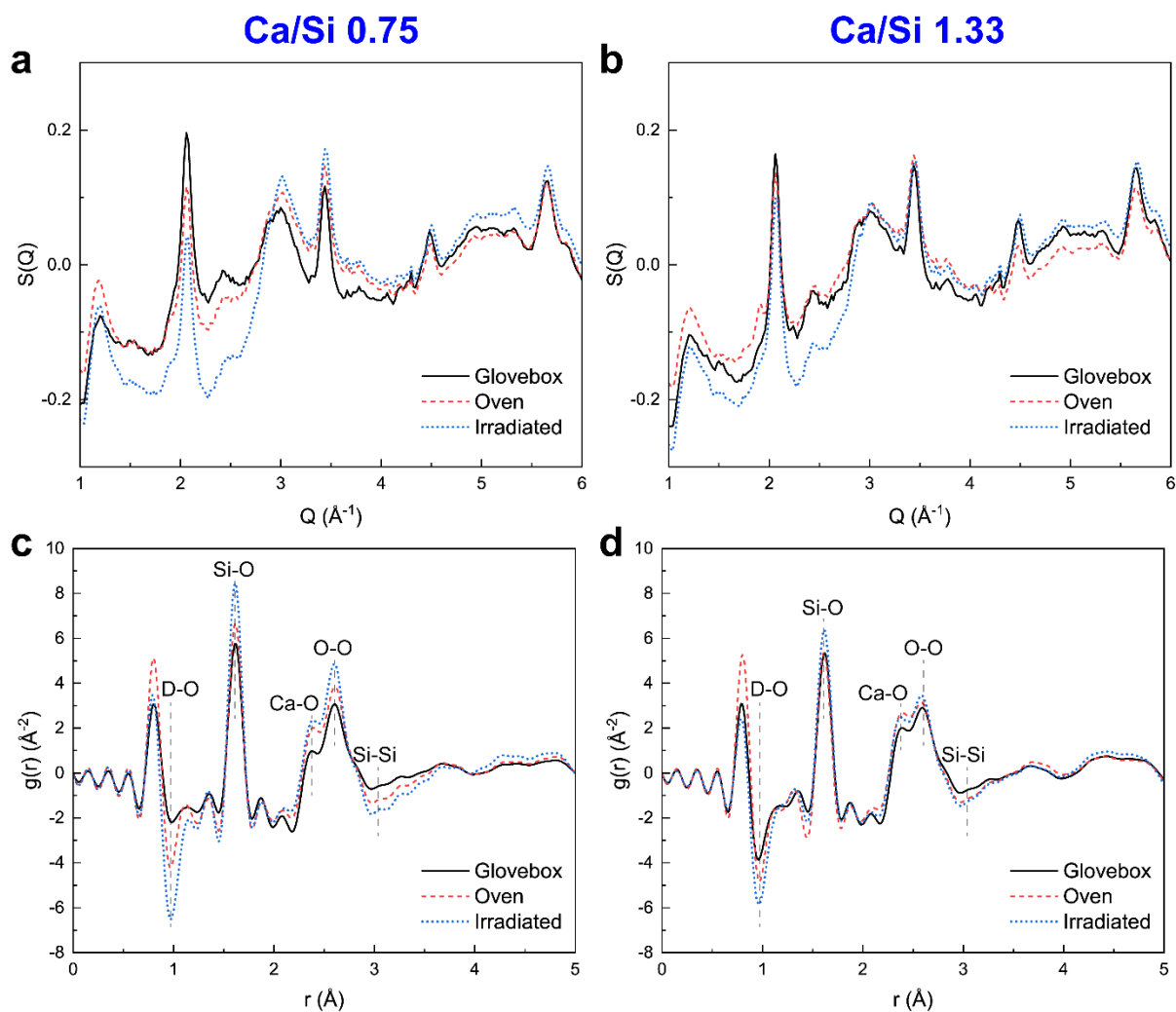


Figure 12. Neutron total scattering patterns of C-S-D gels with (a) Ca/Si of 0.75 and (b) Ca/Si of 1.33. The C-S-D samples were kept in the glovebox (black line), oven-dried (red dashed), and gamma- and neutron-irradiated (blue dotted). (c) and (d) show the pair distribution function of C-S-D gels with Ca/Si of 0.75 and 1.33, respectively.

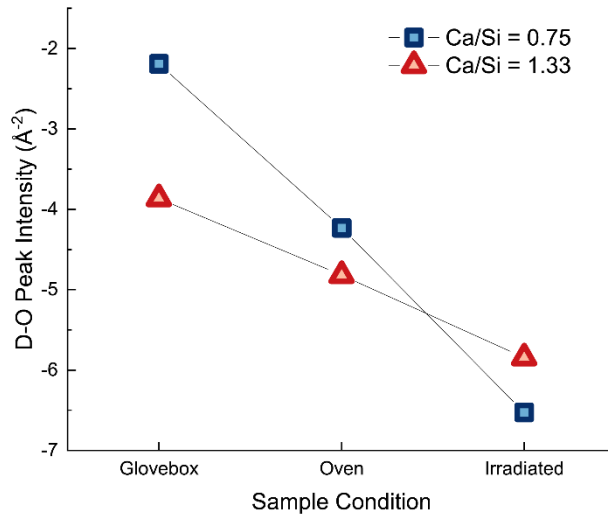


Figure 13. D-O peak intensity (at $\sim 0.95 \text{ \AA}$) obtained from the neutron PDF data of C-S-D samples with different conditions.

6. CONCLUSIONS

An irradiation experiment was designed and executed in collaboration with the Centrum Vizkumu ReŽ in the Czech Republic. C-S-D specimens with Ca/Si ratios of 0.75 and 1.33 were irradiated for approximately 2 years in an out-of-core position in the LVR-15 test reactor to achieve approximately 10^{19} n/cm^2 ($E > 0.1 \text{ MeV}$) of fast neutron fluence and 1 GGy of gamma ray dose at approximately 37°C – 52°C . A companion experiment subjecting the specimens to the irradiation temperature was conducted to separate the effects of extended drying at moderate temperature from the combined effects of irradiation and temperature. Pre- and post-irradiation characterization included thermogravimetry to determine the total water content, XRD to determine the interlayer spacing, and total scattering to obtain pair distribution functions to determine the interatomic distances.

The combination of thermogravimetry, total neutron scattering, and pair distribution function analysis has shown that samples with Ca/Si of 1.33 are less susceptible to irradiation damage than samples with Ca/Si of 0.75. Total scattering showed that dehydration occurred from pre-conditioning to thermal heating and further progressed with irradiation, but the effect was less pronounced for the high Ca/Si ratio. Thermogravimetry showed the same effect by comparing heated and irradiated samples.

X-ray diffraction of the irradiated specimens was not possible to obtain due to a large background of the radiological sample containment covering the basal reflection. More powerful sources such as a synchrotron or neutrons are suggested for further investigations. Nanoindentation is also planned to be performed on the specimens to study the effects of irradiation and the subsequent associated dehydration on mechanical properties.

The fact that samples with high Ca/Si ratio are more radiation resistant can be considered when designing new concrete nuclear structures, as blended systems that promote high Ca/Si ratio in C-S-H should behave more favorably in radiation environments.

7. REFERENCES

1. Giorla, A., et al., *Meso-scale modeling of irradiated concrete in test reactor*. Nuclear Engineering and Design, 2015. **295**: p. 59-73.
2. Giorla, A.B., Y. Le Pape, and C.F. Dunant, *A creep-damage model for mesoscale simulations of concrete expansion-degradation phenomena*. CONCREEP-10, 2015: p. 537-540.
3. Giorla, A.B., Y. Le Pape, and C.F. Dunant, *Computing creep-damage interactions in irradiated concrete*. Journal of Nanomechanics and Micromechanics, 2017. **7**(2): p. 04017001.
4. Le Pape, Y., K.G. Field, and I. Remec, *Radiation effects in concrete for nuclear power plants, Part II: Perspective from micromechanical modeling*. Nuclear Engineering and Design, 2015. **282**: p. 144-157.
5. Esselman, T., P. Bruck, and B. Forget, *Expected condition of concrete exposed to radiation at age of 80 years of reactor operation*. 2013, LPI.
6. Kontani, O., et al. *Evaluation of irradiation effects on concrete structure: Gamma-ray irradiation tests on cement paste*. in *ASME 2013 Power Conference*. 2013. American Society of Mechanical Engineers.
7. Remec, I., *Radiation Environment in Concrete Biological Shields of Nuclear Power Plants*, in *Light Water Reactor Sustainability Program*. 2013.
8. Remec, I., et al., *Characterization of Radiation Fields for Assessing Concrete Degradation in Biological Shields of NPPs*, in *9th Topical Meeting of the Radiation Protection and Shielding Division of the American Nuclear Society (RPSD-2016)*. 2016.
9. Field, K.G., I. Remec, and Y. Le Pape, *Radiation effects in concrete for nuclear power plants—Part I: Quantification of radiation exposure and radiation effects*. Nuclear Engineering and Design, 2015. **282**: p. 126-143.
10. Maruyama, I., et al. *Evaluation of Irradiation Effects on Concrete Structure: Background and Preparation of Neutron Irradiation Test*. in *ASME 2013 Power Conference*. 2013. American Society of Mechanical Engineers.
11. Hilloulin, B., M. Robira, and A. Loukili, *Coupling statistical indentation and microscopy to evaluate micromechanical properties of materials: Application to viscoelastic behavior of irradiated mortars*. Cement and Concrete Composites, 2018. **94**: p. 153-165.
12. McDowall, D. *The Effects of Gamma Radiation on the Creep Properties of Concrete*. in *Proceedings of an Information Exchange Meeting on 'Results of Concrete Irradiation Programmes'*. 1971.
13. Baral, A., et al., *Ultra-high gamma irradiation of calcium silicate hydrates: Impact on mechanical properties, nanostructure, and atomic environments*. Cement and Concrete Research, 2022. **158**: p. 106855.
14. Krishnan, N.M.A., et al., *Revealing the Effect of Irradiation on Cement Hydrates: Evidence of a Topological Self-Organization*. ACS Applied Materials & Interfaces, 2017. **9**(37): p. 32377-32385.
15. Alizadeh, R., J.J. Beaudoin, and L. Raki, *Viscoelastic nature of calcium silicate hydrate*. Cement and Concrete Composites, 2010. **32**(5): p. 369-376.
16. Tamtsia, B.T. and J.J. Beaudoin, *Basic creep of hardened cement paste: A re-examination of the role of water*. Cement and Concrete Research, 2000. **30**(9): p. 1465-1475.
17. Ulm, F.J., F. Le Maou, and C. Boulay, *Creep and shrinkage coupling: new review of some evidence*. Revue française de génie civil, 1999. **3**(3-4): p. 21-37.
18. Vandamme, M. and F.-J. Ulm, *Nanogranular origin of concrete creep*. Proceedings of the National Academy of Sciences, 2009. **106**(26): p. 10552-10557.
19. Pignatelli, I., et al., *A dissolution-precipitation mechanism explains the origin of concrete creep in moist environments*. Journal of Chemical Physics, 2016. **145**.
20. Li, X., et al., *Creep and relaxation of cement paste caused by stress-induced dissolution of hydrated solid components*. Journal of the American Ceramic Society, 2018. **101**(9): p. 4237-4255.

21. Moradian, M., M.T. Ley, and Z.C. Grasley, *Stress induced dissolution and time-dependent deformation of portland cement paste*. *Materials & Design*, 2018. **157**: p. 314-325.
22. Hunnicutt, W.A., P. Mondal, and L.J. Struble, *Effect of Aluminum Substitution in C-S-H on Viscoelastic Properties: Stress Relaxation Nanoindentation*, in *1st International Conference on Grand Challenges in Construction Materials*. 2016.
23. Feldman, R.F. and P.J. Sereda, *A new model for hydrated portland cement and its practical implications*. *Engineering Journal*, 1970. **53**: p. 53-59.
24. Tajuelo Rodriguez, E., *Study of the effects of a 25 MGy gamma dose on mechanical and structural properties of cement paste analogues, Light Water Reactor Sustainability Program, ORNL/TM-2018/1011*. 2018.
25. Tajuelo Rodriguez, E. and W.A. Hunnicutt, *Experimental study of the effects of gamma irradiation on relaxation properties of synthesized Calcium-Silicate-Hydrate using the ORNL ⁶⁰Co irradiator, Light Water Reactor Sustainability Program, ORNL/TM-2017/279*. 2017.
26. Hunnicutt, W., et al., *Examination of Gamma-irradiated Calcium Silicate Hydrates. Part II: Mechanical Properties*. *Journal of Advanced Concrete Technology*, 2020. **18**(10): p. 558-570.
27. Tajuelo Rodriguez, E., et al., *Examination of gamma-irradiated calcium silicate hydrates. Part I: Chemical-structural properties*. *Journal of the American Ceramic Society*, 2020. **103**(1): p. 558-568.
28. Tajuelo Rodriguez, E., B. A., and N. Garg, *Study of the effects of a 200 MGy gamma dose on mechanical and structural properties of cement paste analogues, Light Water Reactor Sustainability Program, ORNL/TM-2019/1329*. 2019.
29. White, C.E., *Effects of temperature on the atomic structure of synthetic calcium-silicate-deuterate gels: A neutron pair distribution function investigation*. *Cement and Concrete Research*, 2016. **79**: p. 93-100.
30. Łowińska-Kluge, A. and P. Piszora, *Effect of gamma irradiation on cement composites observed with XRD and SEM methods in the range of radiation dose 0-1409 MGy*. *Acta Physica Polonica-Series A General Physics*, 2008. **114**(2): p. 399.
31. Bykov, G.L., et al., *Gas formation upon γ -irradiation of cement material*. *High Energy Chemistry*, 2008. **42**(3): p. 211-214.
32. Bouniol, P., B. Muzeau, and V. Dauvois, *Experimental evidence of the influence of iron on pore water radiolysis in cement-based materials*. *Journal of Nuclear Materials*, 2013. **437**(1): p. 208-215.
33. Le Caër, S., et al., *Radiolysis of Confined Water: Hydrogen Production at a High Dose Rate*. *ChemPhysChem*, 2005. **6**(12): p. 2585-2596.
34. Rotureau, P., et al., *Radiolysis of Confined Water: Molecular Hydrogen Formation*. *ChemPhysChem*, 2005. **6**(7): p. 1316-1323.
35. Bouniol, P. and E. Bjergbakke, *A comprehensive model to describe radiolytic processes in cement medium*. *Journal of Nuclear Materials*, 2008. **372**(1): p. 1-15.
36. Taylor, H.F.W., *Cement chemistry*. 2nd ed. 1997, London: Thomas Telford.
37. Richardson, I.G., *Tobermorite/jennite- and tobermorite/calcium hydroxide-based models for the structure of C-S-H: applicability to hardened pastes of tricalcium silicate, beta-dicalcium silicate, Portland cement, and blends of Portland cement with blast-fumace slag, metakaolin, or silica fume*. *Cement and Concrete Research*, 2004. **34**(9): p. 1733-1777.
38. Jennings, H.M., *Colloid model of C-S-H and implications to the problem of creep and shrinkage*. *Materials and Structures*, 2004. **37**(265): p. 59-70.
39. Jennings, H.M., *Refinements to colloid model of C-S-H in cement: CM-II*. *Cement and Concrete Research*, 2008. **38**(3): p. 275-289.
40. Powers, T.C., *Structure and physical properties of hardened Portland cement paste*. *Journal of the American Ceramic Society*, 1958. **41**(1): p. 1-6.
41. Richardson, I.G., *The nature of the hydration products in hardened cement pastes*. *Cement & Concrete Composites*, 2000. **22**(2): p. 97-113.

42. Richardson, I.G., *The nature of C-S-H in hardened cements*. Cement and Concrete Research, 1999. **29**(8): p. 1131-1147.
43. Garbev, K., et al., *Cell dimensions and composition of nanocrystalline calcium silicate hydrate solid solutions. Part 1: Synchrotron-based X-ray diffraction*. Journal of the American Ceramic Society, 2008. **91**(9): p. 3005-3014.
44. Richardson, I.G., *Model Structures for C-(A)-S-H(I)*. Acta Crystallographica Section B-Structural Science, 2014. **70**: p. 903-923.
45. Skibsted, J., H.J. Jakobsen, and C. Hall, *Direct observation of aluminium guest ions in the silicate phases of cement minerals by Al-27 MAS NMR-Spectroscopy*. Journal of the Chemical Society-Faraday Transactions, 1994. **90**(14): p. 2095-2098.
46. Gartner, E., I. Maruyama, and J. Chen, *A new model for the C-S-H phase formed during the hydration of Portland cements*. Cement and Concrete Research, 2017. **97**: p. 95-106.
47. Alizadeh, R., J.J. Beaudoin, and L. Raki, *Mechanical properties of calcium silicate hydrates*. Materials and Structures, 2011. **44**(1): p. 13-28.
48. Bentur, A., et al., *Creep and drying shrinkage of calcium silicate pastes IV. Effects of accelerated curing*. Cement and Concrete Research, 1979. **9**(2): p. 161-169.
49. Le Pape, Y., et al. *Effects of neutron irradiation on the bond strength of steel embedded in concrete*. in *Transactions of the SMIRT 27*. 2024.
50. Degen, T., et al., *The HighScore suite*. 2014. **29**(Supplement S2): p. S13-S18.
51. Tajuelo Rodriguez, E., et al., *Thermal stability of C-S-H phases and applicability of Richardson and Groves' and Richardson C-(A)-S-H(I) models to synthetic C-S-H*. Cement and Concrete Research, 2017. **93**: p. 45-56.
52. Warren, B., H. Krutter, and O. Morningstar, *Fourier analysis of X-ray patterns of vitreous SiO₂ and B₂O₂*. Journal of the American Ceramic Society, 1936. **19**(1-12): p. 202-206.
53. Morandea, A.E. and C.E. White, *In situ X-ray pair distribution function analysis of accelerated carbonation of a synthetic calcium-silicate-hydrate gel*. Journal of Materials Chemistry A, 2015. **3**(16): p. 8597-8605.
54. Garg, N. and C.E. White, *Mechanism of zinc oxide retardation in alkali-activated materials: an in situ X-ray pair distribution function investigation*. Journal of Materials Chemistry A, 2017. **5**(23): p. 11794-11804.
55. White, C.E., et al., *In situ synchrotron X-ray pair distribution function analysis of the early stages of gel formation in metakaolin-based geopolymers*. Applied Clay Science, 2013. **73**: p. 17-25.
56. Gong, K. and C.E. White, *Time-dependent phase quantification and local structure analysis of hydroxide-activated slag via X-ray total scattering and molecular modeling*. Cement and Concrete Research, 2022. **151**: p. 106642.
57. Garbev, K., et al., *Cell dimensions and composition of nanocrystalline calcium silicate hydrate solid solutions. Part 2: X-ray and thermogravimetry study*. Journal of the American Ceramic Society, 2008. **91**(9): p. 3015-3023.
58. Józwiak-Niedźwiedzka, D., et al., *Effect of gamma irradiation on the mechanical properties of carbonation reaction products in mortar*. Materials and Structures, 2022. **55**(6): p. 164.
59. Maruyama, I., et al., *Impact of gamma-ray irradiation on hardened white Portland cement pastes exposed to atmosphere*. Cement and Concrete Research, 2018. **108**: p. 59-71.
60. Cong, X. and R.J. Kirkpatrick, *²⁹Si NMR study of the structure of calcium silicate hydrate*. Advanced Cement Based Materials, 1996. **3**(3:4): p. 144-156.
61. Roosz, C., et al., *Distribution of Water in Synthetic Calcium Silicate Hydrates*. Langmuir, 2016. **32**(27): p. 6794-6805.
62. Yin, C., et al., *Influence of calcium to silica ratio on H₂ gas production in calcium silicate hydrate*. Radiation Physics and Chemistry, 2019. **162**: p. 66-71.
63. Hunnicutt, W.A., *Influence of calcium-(alumino)-silicate-hydrate nanostructure on viscoelastic behavior*. 2018, University of Illinois at Urbana-Champaign.
64. Soper, A. and C. Benmore, *Quantum differences between heavy and light water*. Physical review

letters, 2008. **101**(6): p. 065502.

